Magnon dark mode of an antiferromagnetic insulator in a microwave cavity

Y. Xiao,[1] X. H. Yan,[1,2] Y. Zhang,[1] V. L. Grigoryan,[3] C. M. Hu,[4] H. Guo,[5] and K. Xia[3]
[1]*College of Science, Nanjing University of Aeronautics and Astronautics, Nanjing 210016, China*
[2]*School of Material Science and Engineering, Jiangsu University, Zhenjiang 212013, China*
[3]*The Center for Advanced Quantum Studies and Department of Physics, Beijing Normal University, Beijing 100875, China*
[4]*Department of Physics and Astronomy, University of Manitoba, Winnipeg, Canada R3T 2N2*
[5]*Department of Physics, McGill University, Montreal, Quebec, Canada H3A 2T8*

(Received 3 January 2018; revised manuscript received 31 October 2018; published 6 March 2019)

Magnon dark mode, which possesses long coherence time, has been observed in transmission experiments of a microwave cavity loaded with two yttrium iron garnet spheres. Due to two sublattice magnetizations, it seems likely to exhibit magnon dark mode in an isolated antiferromagnet (AFM). To demonstrate such possibility, we developed two distinct approaches based on the magnon-photon Hamiltonian of AFM-embedded cavity and the transfer matrix method, respectively. The numerical and analytical results show that the magnon dark mode can not be obtained in AFM due to different mode polarization of two magnon modes for propagation parallel to applied field and unequal frequencies for propagation perpendicular to applied field. Contrary to previous theoretical work, our calculation includes both mode polarization and propagation direction of waves explicitly, which are important for correctly describing the coupling between cavity photons and AFM magnons. Moreover, it is found that the cavity resonance remains unperturbed even when the magnon-photon coupling is present. This behavior is attributed to the competition between two types of magnon-photon interactions. The results reported here are important for understanding cavity optomagnonics in AFM, ferrimagnet, and other magnets with multiple sublattice magnetizations.

DOI: 10.1103/PhysRevB.99.094407

I. INTRODUCTION

Thanks to the rapid progress in the field of quantum information, diverse quantum phenomena have been revealed for the coupling between photon and atom, spin, and superconducting qubit [1–12]. In order to achieve both strong coupling and long coherent time, the advances in hybrid quantum systems have given rise to remarkable progress [13–17], especially in the field of spin-photon interaction [18,19]. Due to the fact that all spins in a ferromagnet are aligned by strong exchange interaction, the collective excitation, i.e., magnon, has become a potential candidate for application in hybrid quantum devices. Strong coupling between cavity photon and magnon (cavity magnon polariton) has been observed at both low and high temperatures [20–31], as well as magnetically induced transparency and the Purcell effects, etc. [32].

Strong coupling between cavity photon and magnon verified by some experiments to date is a key factor for realizing the magnon-based hybrid quantum manipulations. However, the resonance nature of the magnon-photon interaction causes extra damping in addition to the intrinsic damping of ferromagnet, which deteriorates the coherence time of the system. One of the possible solutions, proposed recently by Zhang *et al.* [33], is to exploit the magnon dark mode, which is the coherent superposition state of multiple magnon modes. Under certain conditions, the spin precessions in two or more magnons are out of phase and thus destructive interference dominates the interaction which reproduces the dark state of magnons. An important property of magnon dark mode is that it is decoupled from the cavity mode and thus preserves long coherence time. In the experiment of Zhang *et al.* [33], several independent yttrium iron garnet (YIG) spheres are loaded in the microwave cavity and the magnon dark mode is clearly obtained. However, the rapid tuning of magnon frequency of each YIG sphere becomes a serious problem [33], which limits the potential application for quantum manipulation. In an antiferromagnet (AFM), there are two different magnon modes which seem likely to exhibit magnon dark mode. Recently, Yuan and Wang studied the magnon-photon coupling in an AFM-embedded cavity theoretically [34]. The Hamiltonian derived in Ref. [34] shows that two magnon modes of AFM can couple with a common photon mode, which implies that the magnon dark mode is possible to appear. However, the mode polarization and propagation direction of electromagnetic wave, which are important to correctly describe the magnon modes of AFM [35–37], are not involved. Therefore, it is still necessary to carry out a further and systematic study on the cavity magnon polariton of AFM.

Moreover, very recently, Johansen and Brataas studied the cavity-mediated coupling between ferromagnetic resonance (FMR) and antiferromagnetic resonance (AFMR) [38]. This work focused on one of two AFMR magnon modes and discussed strong coupling between this mode and FMR mode, which provides considerable insights into the strength and mechanisms of magnon-magnon coupling. However, the magnon dark mode of an AFM, which is the main result of our paper, has not been studied in Ref. [38].

In this paper, we studied the possibility of creating magnon dark mode in an AFM insulator based on both semiclassical and classical methods. The semiclassical method is

based on the Hamiltonian of an AFM-embedded cavity which is obtained by first diagonalizing the magnetic Hamiltonian to obtain magnon modes and then deriving the Hamiltonian for magnon-photon coupling. The second method, i.e., the classical method, is the transfer matrix method which solves for the microwave transmission through multiple magnetic/nonmagnetic layers [39–41]. Both methods, in which the mode polarization and propagation direction are considered explicitly, reproduce physically consistent results.

The remainder of this paper is organized as follows. In Sec. II, we provide a comprehensive description of transfer matrix method and the Hamiltonian method for cavity magnon polariton of AFM. Section III is devoted to the analysis of numerical results of microwave transmission coefficient. The magnon dark mode is discussed based on both numerical and analytical results. We discussed the difference in method and physics between our work and a similar work published recently [34]. Moreover, we studied a regime in which the cavity resonance is not affected by magnon-photon interaction due to the competition between two types of magnon-photon interactions. Finally, we conclude our findings in Sec. IV.

II. THEORY AND METHOD

In order to study cavity magnon polariton of AFM, we consider two theoretical methods. The first one is the transfer matrix method which has been widely used to deal with the propagation of electromagnetic wave [35–37]. To do so, we solve the Maxwell's equations and the Landau-Lifshitz-Gilbert (LLG) equation simultaneously to give the propagation state. Then, the transfer matrix is built up and the transmission coefficient of an AFM-loaded microwave cavity is calculated carefully. The second method used in this paper is the Hamiltonian method which is implemented by deriving the Hamiltonian with pure magnetic interaction, pure photon field, and magnon-photon interaction. In these two methods, the numerical results are obtained based on the transfer matrix method since it considers realistic cavity geometry and AFM material specifics. The derived Hamiltonian is used to provide physical explanation and analysis to numerical results. Therefore, the values of parameters in the Hamiltonian are not given explicitly.

A. Transfer matrix method

The dynamics of two sublattice magnetizations ($\vec{M}_{A,B}$) in an AFM is described by the LLG equations [42–46]

$$\frac{d\vec{M}_{A,B}}{dt} = -\gamma\vec{M}_{A,B}\times(\vec{H}_{\text{eff}}+\vec{h}) + \alpha_G\vec{M}_{A,B}\times\frac{d\vec{M}_{A,B}}{dt}, \quad (1)$$

where $\vec{h}$ is the microwave magnetic field, α_G is the Gilbert damping rate, and γ is the gyromagnetic ratio. The effective magnetic field is $\vec{H}_{\text{eff}}^{(A,B)} = H_0\vec{y} \pm H_A\vec{y} - \lambda\vec{M}_{B,A}$ for each sublattice magnetization. Here, H_0, H_A, and $H_E = \lambda M_0$ are the static magnetic field, anisotropy field, and exchange field. $|\vec{M}_A| = |\vec{M}_B| = M_0$ is the saturation magnetization. λ describes the exchange coupling strength between sublattice magnetizations A and B.

Under the small-angle precession approximation, we can linearize the above LLG equations. Due to the presence of two sublattice magnetizations, we need to consider the total dynamic magnetization, i.e., $\vec{m} = \vec{m}_A + \vec{m}_B$, to construct the magnetic susceptibility tensor. Here, only the dynamic magnetization ($m_{x,z}$) is given. The linearization of the LLG equation gives rise to

$$\begin{pmatrix} m_x \\ m_z \end{pmatrix} = \begin{pmatrix} \chi_L & i\chi_T \\ -i\chi_T & \chi_L \end{pmatrix}\begin{pmatrix} h_x \\ h_z \end{pmatrix}, \quad (2)$$

where the longitudinal and transverse susceptibilities take the form of

$$\chi_{L,T} = \frac{\gamma M_0(\gamma H_A - i\alpha_G\omega)}{\omega_0^2 - (\omega+\gamma H_0)^2} \pm \frac{\gamma M_0(\gamma H_A - i\alpha_G\omega)}{\omega_0^2 - (\omega-\gamma H_0)^2}. \quad (3)$$

Here, $\omega_0^2 = (\gamma H_A - i\alpha_G\omega)(\gamma H_A + 2\gamma H_E - i\alpha_G\omega)$. In the absence of damping, the susceptibilities reduce to the familiar form given by Mills and Burstein [47].

Next, we introduce the Maxwell's equations

$$\nabla\times\vec{e} = -\frac{\partial\vec{b}}{\partial t} = -\mu_0\frac{\partial(\vec{h}+\vec{m})}{\partial t}, \quad (4)$$

$$\nabla\times\vec{h} = \epsilon_0\epsilon_r\frac{\partial\vec{e}}{\partial t}, \quad (5)$$

where $\vec{e}$, $\vec{b}$, $\vec{h}$, and $\vec{m}$ are electric field, magnetic induction, magnetic field, and dynamic magnetization. μ_0, ϵ_0, and ϵ_r are vacuum permeability, vacuum permittivity, and relative permittivity.

Eliminating the electric field $\vec{e}$ and substituting Eq. (2) into the Maxwell's equations, we obtain two equations for $h_{x,z}$. The forms of these two equations depend on the angle between the static magnetic field $\vec{H}_0$ and propagation direction $\vec{k}$. As $\vec{H}_0 \parallel \vec{k}$, we have

$$\begin{pmatrix} (1+\chi_L)k_0^2 - k^2 & i\chi_T k_0^2 \\ -i\chi_T k_0^2 & (1+\chi_L)k_0^2 - k^2 \end{pmatrix}\begin{pmatrix} h_x \\ h_z \end{pmatrix} = 0 \quad (6)$$

with $k_0^2 = \epsilon_0\epsilon_r\mu_0\omega^2$. Letting the determinant be zero gives rise to two solutions of k, i.e.,

$$k_\pm^2 = (1+\chi_L \pm \chi_T)k_0^2. \quad (7)$$

By analyzing the eigenvectors of Eq. (6), we find that k_+ and k_- correspond to pure right and left circularly polarized states, respectively. Moreover, these pure circularly polarized states of AFM are different from those of ferromagnetic material in which only the k_+ state is allowed to propagate. This is because only the right circularly polarized state k_+ is excited as $\vec{H}_0$ is along the $+\vec{y}$ [48]. But, for an AFM, both right and left circularly polarized states are excited for an applied field and, therefore, the k_- state does contribute to the magnon-photon coupling.

As $\vec{H}_0 \perp \vec{k}$, we obtain only one propagation state

$$k^2 = \frac{(1+\chi_L)^2 - \chi_T^2}{1+\chi_L}k_0^2. \quad (8)$$

The analysis of eigenvector shows that this state is elliptically polarized. With the propagation states k, we can write the

transfer matrix equation [26]

$$\begin{pmatrix} e_y^d \\ h_x^d \end{pmatrix} = \begin{pmatrix} \cos(kd) & iZ\sin(kd) \\ i\frac{1}{Z}\sin(kd) & \cos(kd) \end{pmatrix} \begin{pmatrix} e_y^0 \\ h_x^0 \end{pmatrix} \tag{9}$$

which connects the electric/magnetic fields at one surface ($z = 0$) and those at another surface ($z = d$). $Z = \frac{\mu_0\mu_s\omega}{k}$ is impedance and the effective permeability μ_s is determined by $k = \frac{\omega}{c}\sqrt{\epsilon_r\mu_s}$.

After the transfer matrix is constructed, we can now solve for the problem of microwave propagation in an AFM-loaded cavity and obtain the microwave transmission coefficient S_{21}. In the calculations, a well-designed microwave cavity with circular waveguide and two circular-rectangular transitions at each end of waveguide are used. Such a cavity has been used in cavity magnon polariton experiments of YIG [26]. The length of cavity is 85.0 mm. In the transition region, the microwave in the circular waveguide is strongly reflected and thus a standing wave forms inside the cavity. The reflection coefficient is 0.997 and the phase change due to the reflection is 215°. The difference between the orientations of left and right rectangular waveguides is described by θ which equals 45° in our calculations. These parameters reproduce the observed cavity resonance frequency in experiment. The thickness of AFM layer is 0.5 mm and the relative permittivity is 15.0. More details of method and cavity geometry can be found in Ref. [26].

B. Magnon-photon coupling Hamiltonian

In order to explain numerical results and make physics more transparent, we derive a magnon-photon coupling Hamiltonian for an AFM in cavity. The Hamiltonian consists of three terms, i.e., the magnon, photon, and magnon-photon interactions.

1. Magnon Hamiltonian

In the theory, we express two sublattice magnetizations of AFM by field variable $\vec{M}_{A,B}(\vec{r})$. Such a treatment has been used in the derivation of Hamiltonian for ferromagnetic system [49]. The magnon Hamiltonian consists of four types of interaction, i.e., the exchange, anisotropy, Zeeman, and magnetostatic energy.

We first discuss the exchange interaction in an AFM and write the exchange energy density as

$$\mathcal{H}_{ex} = J\vec{M}_A(\vec{r}) \cdot \vec{M}_B(\vec{r}), \tag{10}$$

where J is the exchange constant. To proceed, we introduce the Holstein-Primakoff (HP) transformation [50] for magnetization $M^{\pm}(\vec{r}) = M_x(\vec{r}) \pm iM_y(\vec{r})$:

$$M_A^+(\vec{r}) = \sqrt{2g\mu_B M_0}\sum_k e^{-i\vec{k}\cdot\vec{r}}a_k,$$

$$M_B^+(\vec{r}) = \sqrt{2g\mu_B M_0}\sum_k e^{i\vec{k}\cdot\vec{r}}b_k^\dagger,$$

$$M_A^-(\vec{r}) = \sqrt{2g\mu_B M_0}\sum_k e^{i\vec{k}\cdot\vec{r}}a_k^\dagger,$$

$$M_B^-(\vec{r}) = \sqrt{2g\mu_B M_0}\sum_k e^{-i\vec{k}\cdot\vec{r}}b_k,$$

$$M_A^z(\vec{r}) = M_0 - g\mu_B\sum_{k,k'} e^{i(\vec{k}-\vec{k'})\cdot\vec{r}}a_k^\dagger a_{k'},$$

$$M_B^z(\vec{r}) = -M_0 + g\mu_B\sum_{k,k'} e^{i(\vec{k}-\vec{k'})\cdot\vec{r}}b_k^\dagger b_{k'}, \tag{11}$$

where g is the g factor and μ_B is the Bohr magneton. In the HP transformation, only the lowest-order term is kept and all other high-order terms are omitted under the small-angle precession approximation.

Substituting the HP transformation into Eq. (10) and integrating the exchange energy density, we obtain the Hamiltonian of exchange interaction

$$H_{ex} = \int \mathcal{H}_{ex}d\vec{r} = w_{ex}\sum_k [a_k b_{-k} + a_k^\dagger b_{-k}^\dagger + b_k^\dagger b_k + a_k^\dagger a_k], \tag{12}$$

where $w_{ex} = g\mu_B J$.

Similarly, we write the Zeeman energy density as $\mathcal{H}_z = -H_0[M_A^z(\vec{r}) + M_B^z(\vec{r})]$ and obtain the Hamiltonian of Zeeman interaction

$$H_z = g\mu_B H_0\sum_k [a_k^\dagger a_k - b_k^\dagger b_k]. \tag{13}$$

The anisotropy energy density is $\mathcal{H}_a = \frac{K}{M_0^2}[(M_{Ax}^2 + M_{Ay}^2) + (M_{Bx}^2 + M_{By}^2)]$ and thus the anisotropy Hamiltonian is written as

$$H_a = w_a\sum_k [a_k^\dagger a_k + b_k^\dagger b_k], \tag{14}$$

where $w_a = \frac{g\mu_B K}{M_0}$ with the anisotropy constant K.

Another important effect is the magnetostatic interaction in which the demagnetizing field is written as

$$\vec{H}_{de} = -\frac{4\pi\vec{k}\cdot\vec{m}}{k^2}\vec{k}, \tag{15}$$

where $\vec{m} = (M_{Ax}\vec{x} + M_{Ay}\vec{y}) + (M_{Bx}\vec{x} + M_{By}\vec{y})$. As $\vec{k} \parallel \vec{H}_0$, i.e., $\vec{k} \perp \vec{m}$, the demagnetizing field vanishes. Hence, the magnon Hamiltonian is expressed by

$$H_m^{\text{para}} = H_{ex} + H_z + H_a = \sum_k (w_{ex} + w_a + g\mu_B H_0)a_k^\dagger a_k + (w_{ex} + w_a - g\mu_B H_0)b_k^\dagger b_k + w_{ex}(a_k b_{-k} + a_k^\dagger b_{-k}^\dagger). \tag{16}$$

In order to decouple the operators a and b, we implement the Bogoliubov transformation [49]

$$a_k = u\alpha_k + v\beta_{-k}^\dagger,$$
$$b_{-k} = u\beta_{-k} + v\alpha_k^\dagger \tag{17}$$

with

$$u^2(v^2) = \frac{w_{ex} + w_a}{2\sqrt{w_a^2 + 2w_{ex}w_a}} \pm \frac{1}{2}. \tag{18}$$

The diagonalized Hamiltonian is

$$H_m^{\text{para}} = \sum_k [\epsilon_+^{\text{para}} \alpha_k^\dagger \alpha_k + \epsilon_-^{\text{para}} \beta_k^\dagger \beta_k] \tag{19}$$

with magnon energy $\epsilon_\pm^{\text{para}} = \sqrt{w_a^2 + 2w_a w_{ex}} \pm g\mu_B H_0$.

As $\vec{k} \perp \vec{H}_0$, the demagnetizing field in Eq. (15) reproduces the magnetostatic energy, i.e., $H_d = -\frac{1}{2}\vec{H}_{de} \cdot (\vec{M}_A + \vec{M}_B)$. For convenience, we consider the wave vector along the x direction. Then, the magnon Hamiltonian $H_m^{\text{perp}} = H_{ex} + H_z + H_a + H_d$ is written as

$$\begin{aligned} H_m^{\text{perp}} = & \sum_k (w_{ex} + w_a + 2w_d + g\mu_B H_0) a_k^\dagger a_k \\ & + (w_{ex} + w_a + 2w_d - g\mu_B H_0) b_k^\dagger b_k \\ & + (w_{ex} + 2w_d)(a_k b_{-k} + a_k^\dagger b_{-k}^\dagger) + 2w_d (a_k b_k^\dagger + a_k^\dagger b_k) \\ & + w_d (a_k a_{-k} + a_k^\dagger a_{-k}^\dagger) + w_d (b_k b_{-k} + b_k^\dagger b_{-k}^\dagger), \end{aligned} \tag{20}$$

where $w_d = \pi g \mu_B M_0$.

In order to diagonalize H_m^{perp}, we introduce an operator transformation [51]

$$\begin{pmatrix} a_k \\ b_k \\ a_{-k}^\dagger \\ b_{-k}^\dagger \end{pmatrix} = F \begin{pmatrix} \alpha_k \\ \beta_k \\ \alpha_{-k}^\dagger \\ \beta_{-k}^\dagger \end{pmatrix}, \tag{21}$$

where F is a 4×4 matrix, the detailed form of which is determined by obtaining the diagonalized Hamiltonian

$$H_m^{\text{perp}} = \sum_k [\epsilon_+^{\text{perp}} \alpha_k^\dagger \alpha_k + \epsilon_-^{\text{perp}} \beta_k^\dagger \beta_k]. \tag{22}$$

The form of eigenenergy $\epsilon_\pm^{\text{perp}}$ is cumbersome and will not be presented here. But, as $H_0 = 0$, the eigenenergy can be expressed in a simple form

$$\begin{aligned} \epsilon_-^{\text{perp}} &= \sqrt{w_a^2 + 2w_a w_e}, \\ \epsilon_+^{\text{perp}} &= \sqrt{w_a^2 + 2w_a w_e + 8w_a w_d}, \end{aligned} \tag{23}$$

which are the same as those published previously [47].

2. Photon Hamiltonian

In order to reproduce the bare photon Hamiltonian, we introduce the vector potential

$$\vec{A} = A_0 \Sigma_{\lambda=L,R} (\vec{e}_\lambda a_\lambda e^{i\vec{k}\cdot\vec{r}} + \vec{e}_\lambda^* a_\lambda^\dagger e^{-i\vec{k}\cdot\vec{r}}), \tag{24}$$

where A_0 is the amplitude of vector potential. $a_{L,R}$ ($a_{L,R}^\dagger$) represents the creation (annihilation) operator of left (right) circularly polarized photons. The unit vectors $\vec{e}_{L,R} = (\mp\vec{x} - i\vec{y})/\sqrt{2}$.

Based on the quantization of the electromagnetic field, we obtain the photon Hamiltonian

$$H_{ph} = \hbar\omega_a a_L^\dagger a_L + \hbar\omega_a a_R^\dagger a_R. \tag{25}$$

Here, the polarization of photon is given explicitly. We do so because two magnon modes of AFM are polarized. For example, as $\vec{k} \parallel \vec{H}_0$, the α and β modes are left and right circularly polarized, respectively. The requirement of spin angular momentum conservation results in the fact that the polarizations of both photon and magnon should be the same in magnon-photon interaction. However, we usually do not designate the mode polarization in FMR. This is because the polarization of FMR mode is definite when the static magnetic field is fixed. For example, the FMR mode is right circularly polarized as $\vec{H}_0 \parallel \vec{z}$.

3. Magnon-photon Hamiltonian

Finally, we discuss the magnon-photon coupling and derive the coupling Hamiltonian. The first step is to give the form of microwave magnetic field based on the relation $\vec{h} = \nabla \times \vec{A}$. Then, we define the coupling energy density as $\mathcal{H}_{mp} = -\vec{h} \cdot (\vec{M}_A + \vec{M}_B)$ and integrate the energy density to give the coupling Hamiltonian. In the derivation, two types of transformations, i.e., Eqs. (17) and (21), are used.

As $\vec{k} \parallel \vec{H}_0$, the coupling Hamiltonian is

$$H_{mp}^{\text{para}} = (u + v)\left(H_{\text{RWA}}^{\text{para}} + H_{CR}^{\text{para}}\right), \tag{26}$$

where u and v are the transformation coefficients determined by Eq. (18). Here,

$$H_{\text{RWA}}^{\text{para}} = g_0 \sum_k [(a_R \beta_{-k}^\dagger + a_R^\dagger \beta_{-k}) + (a_L \alpha_{-k}^\dagger + a_L^\dagger \alpha_{-k})] \tag{27}$$

describes the resonant magnon-photon interaction while

$$H_{CR}^{\text{para}} = g_0 \sum_k [(a_R \alpha_k + a_R^\dagger \alpha_k^\dagger) + (a_L \beta_k + a_L^\dagger \beta_k^\dagger)] \tag{28}$$

describes the off-resonant interaction. In Eqs. (27) and (28), $g_0 = h_0 \sqrt{g\mu_B M_0}$ with h_0 the amplitude of microwave magnetic field.

As $\vec{k} \perp \vec{H}_0$, the coupling Hamiltonian also consists of resonant and off-resonant parts, i.e.,

$$\begin{aligned} H_{\text{RWA}}^{\text{perp}} = & g_0 \sum_k \{a_R[(F_{13} + F_{43})\alpha_{-k}^\dagger + (F_{14} + F_{44})\beta_{-k}^\dagger] \\ & + \text{H.c.}\} + \{a_L[(F_{23} + F_{33})\alpha_{-k}^\dagger \\ & + (F_{24} + F_{34})\beta_{-k}^\dagger] + \text{H.c.}\} \end{aligned} \tag{29}$$

and

$$\begin{aligned} H_{CR}^{\text{perp}} = & g_0 \sum_k \{a_R[(F_{11} + F_{41})\alpha_k + (F_{12} + F_{42})\beta_k] + \text{H.c.}\} \\ & + \{a_L[(F_{21} + F_{31})\alpha_k + (F_{22} + F_{32})\beta_k] + \text{H.c.}\}, \end{aligned} \tag{30}$$

where F_{ij} is the matrix element in the ith row and jth column of the matrix F in Eq. (21).

It should be noted that the magnon mode under consideration is the AFMR mode, in which one photon excites one magnon and the energy should be conserved. This allows us to work within the rotating-wave approximation (RWA) [12]. That is to say, all terms in H_{CR}^{para} and H_{CR}^{perp} which do not conserve energy can be neglected. Only $H_{\text{RWA}}^{\text{para}}$ and $H_{\text{RWA}}^{\text{perp}}$ are considered in our work. Moreover, we focus on the AFMR mode with a small wave vector and thus will drop the symbol of k in the Hamiltonian from now on.

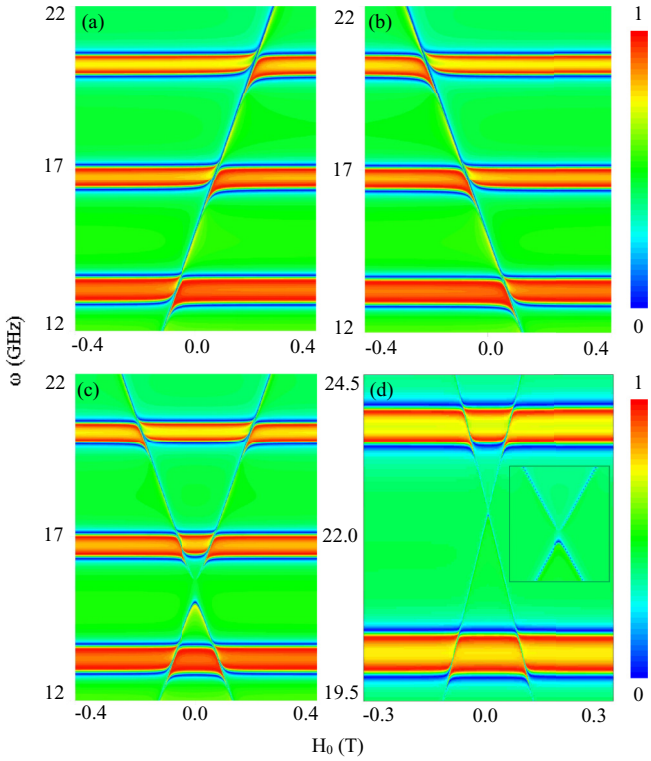

FIG. 1. $|S_{21}|$ spectra of an AFM loaded microwave cavity calculated based on the transfer matrix method. Panels (a) and (b) are for $\vec{k} \parallel \vec{H}_0$ with propagation state k_- and k_+, while (c) and (d) for $\vec{k} \perp \vec{H}_0$. In (a)–(c), the parameters used are $M_0 = 0.15\ T$, $H_A = 0.1\ T$, and $H_E = 1.5\ T$. In (d), the parameters, which are taken from experimental data of $CuCl_2 \cdot 2H_2O$ [58–60], are $M_0 = 0.01\ T$, $H_A = 0.3\ T$, and $H_E = 1.0\ T$. The inset in (d) shows the enlarged region of the crossing point at zero magnetic field.

III. RESULTS AND DISCUSSIONS

Having presented theoretical details, we next show numerical results and the physics behind magnon-photon coupling. Figures 1(a) and 1(b) show the transmission spectra $|S_{21}|$ calculated with the transfer matrix method as $\vec{k} \parallel \vec{H}_0$. In the calculations, the magnon modes in Figs. 1(a) and 1(b) are obtained by selecting the k_- and k_+ states as the propagating state, respectively. Due to the magnon-photon coupling, both α and β modes show characteristic anticrossing features when the cavity resonance crosses the magnon mode. This can be explained based on the above derivation, where the total Hamiltonian is written as

$$H^{\text{para}} = [\omega_a a_R^\dagger a_R + \omega_\beta \beta^\dagger \beta + g(a_R \beta^\dagger + a_R^\dagger \beta)] + [\omega_a a_L^\dagger a_L + \omega_\alpha \alpha^\dagger \alpha + g(a_L \alpha^\dagger + a_L^\dagger \alpha)], \quad (31)$$

where the quantities g_0, u, and v are absorbed into g. For each polarization, we can introduce the transformation $a = A\cos\theta + B\sin\theta$ and $b = B\cos\theta - A\sin\theta$ to diagonalize the Hamiltonian. The eigenenergy is written as

$$\omega = \frac{(\omega_c + \omega_m) \pm \sqrt{(\omega_c - \omega_m)^2 + 4g^2}}{2}. \quad (32)$$

Here, $\cos\theta$ and $\sin\theta$ are coefficients to be determined. $\omega_m = \omega_{\alpha,\beta}$ and $\omega_c = \omega_a$. Equation (32) reproduces the anticrossing features shown in Figs. 1(a) and 1(b) quite well.

Our theory predicts that, despite the existence of two magnon modes in AFM, two types of polarization are completely decoupled. The α (β) magnon mode is excited by the left (right) circularly polarized photon. This indicates that spin angular momentum is conserved in the magnon-photon coupling of AFM. As is known, the magnon dark mode is formed by the simultaneous coupling of two magnon modes with one common photon. Therefore, we will expect that the magnon dark mode will not be obtained in experiments as $\vec{k} \parallel \vec{H}_0$.

Figure 1(c) shows the transmission coefficient as $\vec{k} \perp \vec{H}_0$. In contrast to the case of $\vec{k} \parallel \vec{H}_0$ with two wave vectors $k_\pm$, there is only one propagation state shown in Eq. (8). But, Fig. 1(c) presents two magnon modes. This is because the demagnetizing field mixes two circular polarizations and thus a single propagation state contains information of both magnon modes. In such case, the mode polarization is no longer pure circular, but becomes elliptical. Due to the mixture of two circular polarizations, it seems possible for a photon to couple with two magnon modes simultaneously. To demonstrate the magnon dark mode, we consider a simplified Hamiltonian of Eq. (29):

$$H^D = \hbar\omega_a a^\dagger a + \hbar\omega_\alpha \alpha^\dagger \alpha + \hbar\omega_\beta \beta^\dagger \beta + g_\alpha(a\alpha^\dagger + \alpha a^\dagger) + g_\beta(a\beta^\dagger + \beta a^\dagger), \quad (33)$$

where α ($\alpha^\dagger$), β ($\beta^\dagger$), and a ($a^\dagger$) are the creation (annihilation) operators of two magnons α and β and one cavity photon a. g_α (g_β) is the coupling strength between cavity and two magnon modes. In order to have magnon dark mode, we define two operators

$$B = \frac{g_\alpha \alpha + g_\beta \beta}{G}, \quad (34)$$

$$D = \frac{g_\beta \alpha - g_\alpha \beta}{G} \quad (35)$$

for the bright (B) and dark (D) modes with $G = \sqrt{g_\alpha^2 + g_\beta^2}$. We notice that the above transformation is performed under the small-angle precession approximation, i.e., the deviation of magnetization with respect to static magnetic field is small. This approximation justifies the HP transformation and thus the transformation of bright and dark modes. From an experimental point of view, there are two conditions under which such approximation may be invalid. The first one takes place at high microwave power, which may drive the system into the nonlinear regime. The second one occurs when the magnetic field is high, i.e., the spin-flop transition where the magnetization switches to a direction perpendicular to static magnetic field. In this paper, these two cases are beyond our consideration.

Then, the Hamiltonian, i.e., Eq. (33), is transformed to

$$H_T^D = \hbar\frac{g_\alpha^2\omega_\alpha + g_\beta^2\omega_\beta}{G^2} B^\dagger B + \hbar\frac{g_\alpha^2\omega_\beta + g_\beta^2\omega_\alpha}{G^2} D^\dagger D + \hbar\omega_a a^\dagger a + \frac{g_\alpha g_\beta}{G^2}(\omega_\alpha - \omega_\beta)(B^\dagger D + D^\dagger B) + \hbar G(aB^\dagger + Ba^\dagger). \quad (36)$$

As $\omega_\alpha = \omega_\beta$, the Hamiltonian becomes $H_T^D = \hbar\omega_\alpha B^\dagger B + \hbar\omega_\alpha D^\dagger D + \hbar\omega_a a^\dagger a + \hbar G(aB^\dagger + Ba^\dagger)$. This clearly implies that the dark mode (D) is completely decoupled from the cavity mode. Hence, in order to have magnon dark mode, the condition of $\omega_\alpha = \omega_\beta$ should be satisfied. But, as shown in Fig. 1(c), there appears a frequency splitting between two magnon modes due to the demagnetizing field. We therefore conclude that the magnon dark mode is hard to form due to unequal magnon frequencies as $\vec{k} \perp \vec{H}_0$.

Based on the above analysis, one can see that the demagnetizing field plays an important role in reproducing the frequency splitting at zero magnetic field. Despite the large splitting in Fig. 1(c), it is actually small in realistic AFM materials. As seen in Eq. (23), the demagnetizing field is responsible for the frequency splitting. To measure it, we define a ratio $\frac{\epsilon_+ - \epsilon_-}{\epsilon_-} \approx \frac{w_d}{w_{ex}}$. Taking MnF_2, for example [46], the ratio is estimated to be about 10^{-3}. This indicates that the effect of demagnetizing field on AFMR is small. Therefore, in the case of $\vec{k} \perp \vec{H}_0$, two magnon modes at zero magnetic field are still of circularlike polarizations.

In our calculation, the system under consideration is a thin film and some other material factors are not considered. First, the demagnetizing field gives rise to the frequency splitting as $\vec{k} \perp \vec{H}_0$. This is no longer true for a spheroidal AFM sample. In a magnetized sphere, we can use the demagnetizing tensor to express the demagnetizing field since the calculation based on Eq. (15) becomes complicated [48]. Since the demagnetizing factors are uniform, i.e., $N_x = N_y = N_z$, two magnon modes at zero magnetic field are degenerate and no frequency splitting is present [52–54]. Therefore, the behavior of a spheroidal sample is analogous to the case of $\vec{k} \parallel \vec{H}_0$ of a thin film. Second, the boundary condition is not considered in our paper. We do so because the magnetization precession of AFMR mode is in phase in the entire sample and thus the boundary condition does not play a significant role. In some magnon modes, e.g., standing spin wave, the boundary condition becomes important and needs to be carefully treated [27,55]. Third, the hard-axis anisotropy has been introduced for describing the AFMR in Ref. [38]. As such anisotropy is present in our calculation, it will reproduce a frequency splitting at zero magnetic field and prevents the formation of magnon dark mode.

As mentioned in the Introduction, Yuan and Wang derived a Hamiltonian for an AFM in cavity and diagonalize the Hamiltonian to reproduce the eigenenergy of AFM-cavity system [34]. The derivation in Ref. [34] does not consider the demagnetizing field and thus corresponds to the case of $\vec{k} \parallel \vec{H}_0$ of our work. However, there are obvious differences in the method and physics between our work and Ref. [34]. First, the mode polarization is not explicitly considered in Ref. [34]. This is important since two magnon modes of AFM belong to distinct polarizations. The requirement of spin angular moment conservation dictates the excitation of α (β) magnon mode by left (right) circular photons as $\vec{k} \parallel \vec{H}_0$. If the mode polarization is not included as done in Ref. [34], the derived Hamiltonian will make possible the simultaneous coupling of α and β magnon modes with a common photon. Second, as explained above, it is likely to form magnon dark mode based on the Hamiltonian in Ref. [34]. However, our theory shows that the magnon dark mode can not be obtained due to unequal polarizations as $\vec{k} \parallel \vec{H}_0$ and unequal frequencies as $\vec{k} \perp \vec{H}_0$. Third, the demagnetizing field, which is important for realizing the mixture of α and β magnon modes, is not considered in Ref. [34].

Bose *et al.* [35] and Manohar *et al.* [36] studied the magnon-photon coupling in AFM and calculated the dispersion relation and reflection spectra, respectively. But, both research works did not consider the cavity and thus the physics belongs to magnon polariton, instead of cavity magnon polariton studied here. Moreover, Okuma studied the coupling between cavity photon and nonreciprocal magnon of AFM [56]. The mixture between α and β magnon modes is mediated by the Dzyaloshinskii-Moriya (DM) interaction, instead of the demagnetizing field considered in our work. The magnon-photon coupling is reflected by spin pumping and magnon Bose-Einstein condensate in Ref. [56] while by microwave transmission in our work.

Although the above-mentioned gap between two magnon modes prevents the formation of magnon dark mode, it provides a possibility of exhibiting a type of magnon-photon interaction. Such a feature has not been demonstrated in previous studies of cavity magnon polariton. In Fig. 2, we show the transmission coefficient as $\vec{k} \perp \vec{H}_0$ for various values of H_E. When the exchange field H_E increases, the frequencies of two magnon modes at zero magnetic field increase according to Eq. (23). Here, we focus on the cavity mode at about 16.5 GHz (denoted with red arrow). As $H_E = 1.5\ T$ [Fig. 2(a)], only the upper magnon mode is coupled with the cavity. Due to magnon-photon interaction, the line of cavity resonance bends to lower frequency. In contrast, at $H_E = 1.9\ T$ [Fig. 2(c)], the lower magnon mode crosses the cavity resonance and thus the line of cavity resonance bends to higher frequency. The above two results represent two limiting cases because only one magnon mode dominates the magnon-photon coupling. If the cavity resonance lies within the gap between two magnon modes, it will experience two types of interaction from two magnon modes. These two magnon-photon couplings will compete, which results in the fact that the bend of cavity resonance will depend on the strength of two types of magnon-photon interaction. Under appropriate condition, as shown in Fig. 2(b), two magnon-photon interactions cancel with each other, which makes the cavity resonance almost unperturbed. This provides a means of tuning two types of magnon-photon interactions which are potentially important for magnetic and electromagnetic applications.

Although the cavity magnon polariton of AFM is potentially important, two key concerns for possible AFM materials should be clarified. The first is the damping rate of AFM. If the damping rate is too large to distinguish the anticrossing gap, the strong coupling regime will not be observed in experiment. The second is the high precession frequency of AFM. Unlike the conventional ferromagnetic material, the precession frequency of AFM is in general up to several hundred GHz, e.g., 247 GHz for MnF_2 at 24.7 K and zero magnetic field [57]. However, the resonance frequency of cavity currently used in most of experiments is usually about 10–20 GHz, which makes the resonant coupling between cavity photon and AFM magnons difficult. Here, we propose several possible

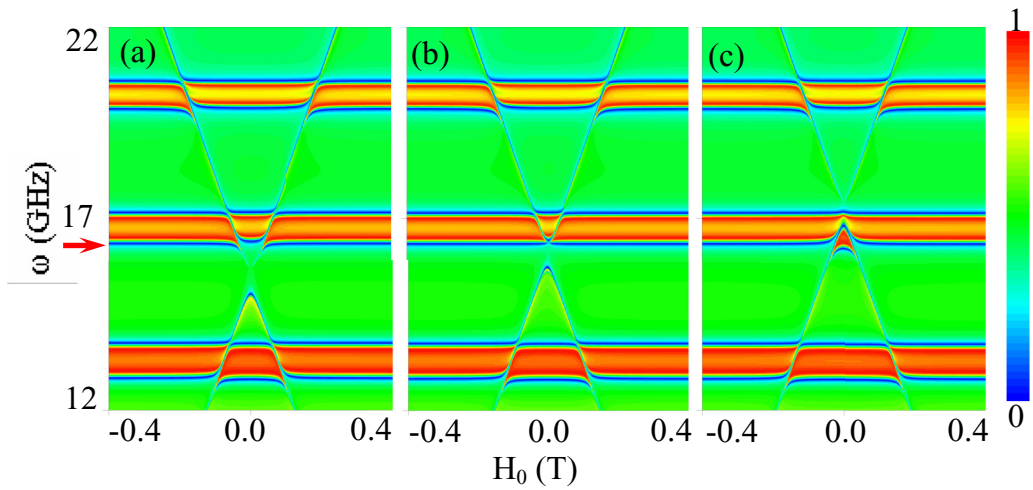

FIG. 2. $|S_{21}|$ spectra of an AFM loaded microwave cavity calculated based on the transfer matrix method with $M_0 = 0.15T$, $H_A = 0.1T$ and (a) $H_E = 1.5T$, (b) $H_E = 1.65T$, (c) $H_E = 1.9T$.

AFM material which could be used to observe the cavity magnon polariton in future experiments. The first is the copper chloride, i.e., $CuCl_2 \cdot 2H_2O$. Gerritsen *et al.* performed antiferromagnetic resonance measurement for a 3-cm-thick sample and found that the resonance field is about 0.3 T at the resonance frequency 9.4 GHz [58,59]. Date's experiment gives rise to the resonance magnetic field of 0.47 T at 9.8 GHz [60]. The linewidth ΔH is very narrow, e.g., 0.086 T, which is comparable to that found in cavity magnon polariton of YIG. Based on experimental data, we estimate the exchange, anisotropy fields, and magnetization which are 1.0, 0.3, and 0.01 T respectively. Figure 1(d) shows the $|S_{21}|$ spectra of $CuCl_2 \cdot 2H_2O$ with the above estimated parameters. It is found that, due to small magnetization, the demagnetizing field induces only a small splitting at zero magnetic field. Moreover, this material is antiferromagnetic in the liquid-helium temperature range, which increases greatly the difficulty in implementing such an ultralow temperature experiment. The second material is the methylaminated potassium fulleride $(CH_3NH_2)K_3C_{60}$ which presents the linewidth $\Delta H = 0.05\ T$ at 9.6 GHz and 15 K, which can meet the strong coupling condition within the microwave frequency range [61]. But, the measurement temperature is still very low. The third possibility is the Cr_2O_3 which shows the linewidth $\Delta H = 0.1\ T$ at 9.3 GHz and room temperature [62,63]. The field parameters are estimated to be $H_A \sim 10^{-2}$ T, $H_E \sim 100$ T, and $M_0 \sim 10^{-2}$ T. Compared to $CuCl_2 \cdot 2H_2O$, Cr_2O_3 has a larger exchange field, which results in a smaller frequency splitting at zero magnetic field.

Finally, we would like to further comment on the spin-flop transition [64,65] usually observed in AFM. Since the cavity resonance frequency is usually within the Ku band of microwave frequency, the magnetic field is low. Moreover, the discussion on magnon dark mode is at zero magnetic field where both magnon modes may have equal frequencies. Although the spin-flop transition can reduce the AFM resonance frequency and resonance field, it is still large for our purpose. It is certainly an interesting topic to discuss the effect of spin-flop transition on the cavity magnon polariton of AFM if the cavity resonance frequency can be promoted to several tens of GHz.

IV. CONCLUSION

In summary, we investigate the cavity magnon polariton of AFM based on two different methods. In the first method, we consider the details of AFM and cavity and derive the transfer matrix for AFM-loaded cavity. Our results show that, as the propagation is parallel to static magnetic field, two circular polarizations are completely decoupled. This makes impossible the coupling of two magnon modes with a common photon mode and magnon dark mode. When the propagation is perpendicular to static magnetic field, the demagnetizing field mixes two polarizations and thus enables the simultaneous coupling of two magnon modes with a photon. However, due to the frequency splitting induced by the demagnetizing field, the magnon dark mode is hard to form. Moreover, the frequency splitting provides a possible means to tune cavity magnon polariton of AFM. As the cavity resonance is inside the gap, it will experience two types of magnon-photon coupling. Under appropriate condition, the cavity resonance remains unperturbed due to the cancellation of two types of magnon-photon interactions. We also discussed several AFM materials which may be used for observing cavity magnon polariton in future experiments.

ACKNOWLEDGMENTS

This work is supported by the National Natural Science Foundation of China (Grants No. NSFC61774017, No. 91750112, and No. 11804158). Y.X. would like to thank Professor G. E. Bauer for his comments in the period of SMEE2017 held in Hong Kong.

[1] C. Cohen-Tannoudji, J. Dupont-Roc, and G. Grynberg, *Atom-photon Interaction* (Wiley, New York, 2004).
[2] S. Haroche, Rev. Mod. Phys. **85**, 1083 (2013).
[3] K. J. Vahala, Nature (London) **424**, 839 (2003).
[4] F. Marquardt, J. P. Chen, A. A. Clerk, and S. M. Girvin, Phys. Rev. Lett. **99**, 093902 (2007).
[5] A. A. Clerk, M. H. Devoret, S. M. Girvin, F. Marquardt, and R. J. Schoelkopf, Rev. Mod. Phys. **82**, 1155 (2010).
[6] L. S. Bishop, J. M. Chow, J. Koch, A. A. Houck, M. H. Devoret, E. Thuneberg, S. M. Girvin, and R. J. Schoelkopf, Nat. Phys. **5**, 105 (2009).
[7] R. H. Dicke, Phys. Rev. **93**, 99 (1954).
[8] M. Tavis and F. W. Cumming, Phys. Rev. **170**, 379 (1968).
[9] M. Tavis and F. W. Cumming, Phys. Rev. **188**, 692 (1969).
[10] G. S. Agarwal, Phys. Rev. Lett. **53**, 1732 (1984).
[11] C. J. Wood, T. W. Borneman, and D. G. Cory, Phys. Rev. Lett. **112**, 050501 (2014).
[12] H. J. Carmichael, *Statistical Methods in Quantum Optics: Non-classical Fields* (Springer, Berlin, 2008).
[13] G. Kurizki, P. Bertet, Y. Kubo, K. Molmer, D. Petrosyan, P. Rabl, and J. Schmiedmayer, Proc. Natl. Acad. Sci. USA **112**, 3866 (2015).
[14] L. Tian, P. Rabl, R. Blatt, and P. Zoller, Phys. Rev. Lett. **92**, 247902 (2004).
[15] J. Q. You and F. Nori, Nature (London) **474**, 589 (2011).
[16] A. Imamoglu, Phys. Rev. Lett. **102**, 083602 (2009).
[17] J. M. Pirkkalainen, Nature (London) **494**, 211 (2013).
[18] I. Chiorescu, N. Groll, S. Bertaina, T. Mori, and S. Miyashita, Phys. Rev. B **82**, 024413 (2010).
[19] A. W. Eddins, C. C. Beedle, D. N. Hendrickson, and J. R. Friedman, Phys. Rev. Lett. **112**, 120501 (2014).
[20] O. O. Soykal and M. E. Flatte, Phys. Rev. Lett. **104**, 077202 (2010).
[21] H. Huebl, C. W. Zollitsch, J. Lotze, F. Hocke, M. Greifenstein, A. Marx, R. Gross, and S. T. B. Goennenwein, Phys. Rev. Lett. **111**, 127003 (2013).
[22] Y. Tabuchi, S. Ishino, T. Ishikawa, R. Yamazaki, K. Usami, and Y. Nakamura, Phys. Rev. Lett. **113**, 083603 (2014).
[23] M. Goryachev, W. G. Farr, D. L. Creedon, Y. Fan, M. Kostylev, and M. E. Tobar, Phys. Rev. Appl. **2**, 054002 (2014).
[24] L. Bai, M. Harder, Y. P. Chen, X. Fan, J. Q. Xiao, and C.-M. Hu, Phys. Rev. Lett. **114**, 227201 (2015).
[25] Y. P. Wang, G. Q. Zhang, D. Zhang, X. Q. Luo, W. Xiong, S. P. Wang, T. F. Li, C.-M. Hu, and J. Q. You, Phys. Rev. B **94**, 224410 (2016).
[26] B. M. Yao, Y. S. Gui, Y. Xiao, H. Guo, X. S. Chen, W. Lu, C. L. Chien, and C.-M. Hu, Phys. Rev. B **92**, 184407 (2015).
[27] Y. Cao, P. Yan, H. Huebl, S. T. B. Goennenwein, and G. E. W. Bauer, Phys. Rev. B **91**, 094423 (2015).
[28] N. J. Lambert, J. A. Haigh, and A. J. Ferguson, J. Appl. Phys. **117**, 053910 (2015).
[29] X. Zhang, C. L. Zou, L. Jiang, and H. X. Tang, Phys. Rev. Lett. **113**, 156401 (2014).
[30] B. M. Yao, Y. S. Gui, J. W. Rao, S. Kaur, X. S. Chen, W. Lu, Y. Xiao, H. Guo, K.-P. Marzlin, and C.-M. Hu, Nat. Commun. **8**, 1437 (2017).
[31] V. L. Grigoryan, K. Shen, and K. Xia, Phys. Rev. B **98**, 024406 (2018).
[32] X. Zhang, C. L. Zou, L. Jiang, and H. X. Tang, Sci. Adv. **2**, e1501286 (2016).
[33] X. Zhang, C. L. Zou, N. Zhu, F. Marquardt, L. Jiang, and H. X. Tang, Nat. Commun. **6**, 8914 (2015).
[34] H. Y. Yuan and X. R. Wang, Appl. Phys. Lett. **110**, 082403 (2017).
[35] S. M. Bose, E. N. Foo, and M. A. Zuniga, Phys. Rev. B **12**, 3855 (1975).
[36] C. Manohar and G. Venkataraman, Phys. Rev. B **5**, 1993 (1972).
[37] K. N. Shrivastava, Phys. Rev. B **19**, 1598 (1979).
[38] O. Johansen and A. Brataas, Phys. Rev. Lett. **121**, 087204 (2018).
[39] G. C. Bailey and C. Vittoria, Phys. Rev. Lett. **28**, 100 (1972).
[40] C. Vittoria, Phys. Rev. B **32**, 1679 (1985).
[41] G. S. Spronken, A. Friedmann, and A. Yelon, Phys. Rev. B **15**, 5141 (1977).
[42] F. Keffer and C. Kittel, Phys. Rev. **85**, 329 (1952).
[43] E. S. Dayhoff, Phys. Rev. **107**, 84 (1957).
[44] R. W. Sanders, V. Jaccarino, and S. M. Rezende, Solid State Commun. **28**, 907 (1978).
[45] T. Okamura, Y. Torizuka, and Y. Kojima, Phys. Rev. **82**, 285 (1951).
[46] F. M. Johnson and A. H. Nethercot, Jr., Phys. Rev. **104**, 847 (1956).
[47] D. L. Mills and E. Burstein, Rep. Prog. Phys. **37**, 817 (1974).
[48] D. D. Stancil and A. Prabhakar, *Spin Wave: Theory and Applications* (Springer, New York, 2009).
[49] C. Kittel, *Quantum Theory of Solids* (Wiley, New York, 1987).
[50] T. Holstein and H. Primakoff, Phys. Rev. **58**, 1098 (1940).
[51] A. Kamra, U. Agrawal, and W. Belzig, Phys. Rev. B **96**, 020411(R) (2017).
[52] R. Loudon and P. Pincus, Phys. Rev. **132**, 673 (1963).
[53] A. Harris, Phys. Rev. **143**, 353 (1966).
[54] H. Yamazaki, E. Soares, H. Panepucci, and Y. Morishige, J. Phys. Soc. Jpn. **47**, 1464 (1979).
[55] H. Jiang, Y. Xiao, C. M. Hu, H. Guo, and K. Xia, Nanotechnology **29**, 254002 (2018).
[56] N. Okuma, arXiv:1805.08226.
[57] F. M. Johnson and A. H. Nethercot, Jr., Phys. Rev. **114**, 705 (1959).
[58] H. J. Gerritsen, M. Garber, and G. W. J. Drewes, Physica (Amsterdam) **22**, 213 (1956).
[59] H. J. Gerritsen, Physica (Amsterdam) **21**, 639 (1955).
[60] M. Date, Phys. Rev. **104**, 623 (1956).
[61] D. Arčon, M. Pregelj, A. Zorko, A. Y. Ganin, M. J. Rosseinsky, Y. Takabayashi, K. Prassides, H. vanTol, and L.-C. Brunel, Phys. Rev. B **77**, 035104 (2008).
[62] E. P. Trounson, D. F. Bleil, R. K. Wangsness, and L. R. Maxwell, Phys. Rev. **79**, 542 (1950).
[63] S. Foner, Phys. Rev. **130**, 183 (1963).
[64] D. J. Simkin and R. A. Bernheim, Phys. Rev. **153**, 621 (1967).
[65] O. Johansen and A. Brataas, Phys. Rev. B **95**, 220408(R) (2017).